Hydroclimatic Variability and Weather Type Characteristics in the Levant During the Last Interglacial

Efraim Bril[1], Adi Torfstein[1,2], Roy Yaniv[1,3], and Assaf Hochman[1]

[1]Fredy and Nadine Herrmann Institute of Earth Sciences, The Hebrew University of Jerusalem, Jerusalem, Israel
[2]Interuniversity Institute for Marine Sciences, Eilat, Israel
[3]Center for Climate Medicine and Human Health, Gertner Institute, Sheba Medical Center, Ramat Gan, Israel

Correspondence: Efraim Bril (efraim.bril@mail.huji.ac.il), Adi Torfstein (adi.torf@mail.huji.ac.il), and Assaf Hochman (Assaf.Hochman@mail.huji.ac.il)

Abstract. Proxy-based reconstructions of the Last Interglacial peak indicate changes in precipitation characteristics in the Levant. These reconstructions suggest that precipitation occurred in brief and intense events, particularly in the region's southern parts. Some studies have offered conflicting paradigms for explaining hydroclimate variability. However, these have yet to be consistently tested in a modeling framework. Indeed, the modeling approach can undoubtedly enhance the combined interpretation of proxy records and our understanding of past hydroclimate processes. We used simulations from the Paleoclimate Model Intercomparison Project 4th phase (PMIP4) to evaluate and reconstruct the precipitation characteristics of the Levant. First, we identify the Alfred Wagner Institute Earth System Model as one that largely resembles proxy reconstructions. Then we used it to understand hydroclimate variability. We examined changes in the frequency, seasonality, and persistence of the Levant's rain-bearing weather types, including Cyprus Lows and Red Sea Troughs. We further decomposed the dynamic and thermodynamic contributions to changes in the water balance, comparing the Last Interglacial peak with Pre-Industrial times. Based on differences in daily mean precipitation, we provide evidence that the rain-bearing weather types yielded significantly more precipitation ($\approx +20\%$) during the Last Interglacial peak. This increase is most evident in the southern Levant, where higher precipitation occurs during Red Sea Trough days, primarily due to thermodynamic changes. Minor differences in the frequency and persistence of these weather types were found. Our research offers insights into historical hydroclimate changes in the Levant, broadening our understanding of future climate impacts driven by natural variability.

1 Introduction

1.1 Overview of climate in the Levant

The hydroclimatic history of the Levant draws attention for two main reasons. First, it lies at the boundary between temperate northern and arid southern climates, rendering it highly responsive to small changes in the large-scale atmospheric circulation (Enzel and Bar-Yosef, 2017). Second, during the Last Interglacial peak, also known as Marine Isotope Stage 5e (MIS 5e), the region experienced conditions that may have enabled humans to migrate "out of Africa." Increased rainfall transformed the otherwise arid area into a viable passage, making it a critical migration gateway for early humans (Bar-Yosef, 1998; Derricourt, 2005; Schwarcz et al., 1988).

The Levant is currently characterized by a Mediterranean-type climate, featuring dry, hot summers and wet, cool winters (Goldreich, 2003; Armon et al., 2019). The precipitation season runs from October to May, with most rainfall occurring during the winter months from December to March (Goldreich, 2003). The average annual rainfall in the northern Levant and mountainous areas exceeds 1000 mm y^{-1} with ≈ 70 rainy days per year (Goldreich, 2003; Armon et al., 2019). In contrast, in the arid southeastern areas, rainfall can be well below 100 mm y^{-1} (Vaks et al., 2007; Armon et al., 2019). These spatial differences are clearly illustrated in Figure 1A, which shows the mean annual rainfall distribution across the Levant for 1980–2020.

The weather types of the Levant have been classified into five main groups, including Cyprus Lows, which are abundant during winter; Red Sea Troughs, which peak in autumn; Persian Troughs, occurring exclusively during summer; high-pressure systems that are present throughout the year; and Sharav Lows, which are prevalent in spring. Cyprus Lows and Red Sea Troughs are the main rain-bearing weather types (Fig. 1 B, C; (Alpert et al., 2004b, a; Hochman et al., 2018c, b; Saaroni et al., 2010; Ziv et al., 2022). Cyprus Lows account for most annual precipitation (80 - 90%) and extreme weather events, while Red Sea Troughs contribute the rest (Goldreich, 2003; Saaroni et al., 2010). Specifically, $\approx 50\%$ of precipitation in the hyper-arid areas of the Levant, such as Eilat, the southernmost city in Israel, is due to the Red Sea Trough weather type (Saaroni et al., 2010; Ziv et al., 2022). In addition to these, the Tropical Plume is considered a rare rain-bearing sub-category that can transport large amounts of moisture from equatorial regions to the Levant (Ziv, 2001; Rubin et al., 2007; Kahana et al., 2002).

The northern Levant is projected to become warmer and drier during the 21st century, associated with a projected decrease in the frequency of the Cyprus Low and Red Sea Trough and associated rainfall, along with significant changes in their seasonal occurrence (Hochman et al., 2018c, b, 2021; Armon et al., 2022). However, more southerly locations are projected to become wetter, with thermodynamic processes proposed as a plausible cause (Hochman et al., 2018d). Extreme precipitation events are projected to be shorter and more intense, with smaller rain areas and higher peak rain rates (Armon et al., 2022).

1.2 Proxy-based hydroclimate reconstruction of the Last Interglacial

The Last Interglacial (LIG) approximately 129-116 ka was characterized by elevated global average temperatures, higher sea levels, and increased atmospheric CO2 concentrations compared to the Pre-Industrial (PI) period (Otto-Bliesner et al., 2021; Dutton and Lambeck, 2012; Govin et al., 2015; Jouzel et al., 2007). During the LIG, the Levant was characterized by a generally dry climate overall (Torfstein et al., 2015, 2013; Kushnir et al., 2024). However, proxy-based reconstructions indicate that during the peak of the LIG ($\sim$127–122 ka), the southern Levant experienced relatively wetter conditions compared to the Pre-Industrial (PI) period, despite remaining dry in absolute terms (Torfstein et al., 2015; Torfstein, 2024). These wetter conditions were characterized by short-lived but high-intensity rainfall events and were spatially confined to the southern Levant, In contrast to the generally arid conditions prevailing across much of the region throughout the LIG. Evidence supporting this interpretation comes from sediment cores obtained from the Dead Sea (Bookman et al., 2006; Waldmann et al., 2009; Torfstein

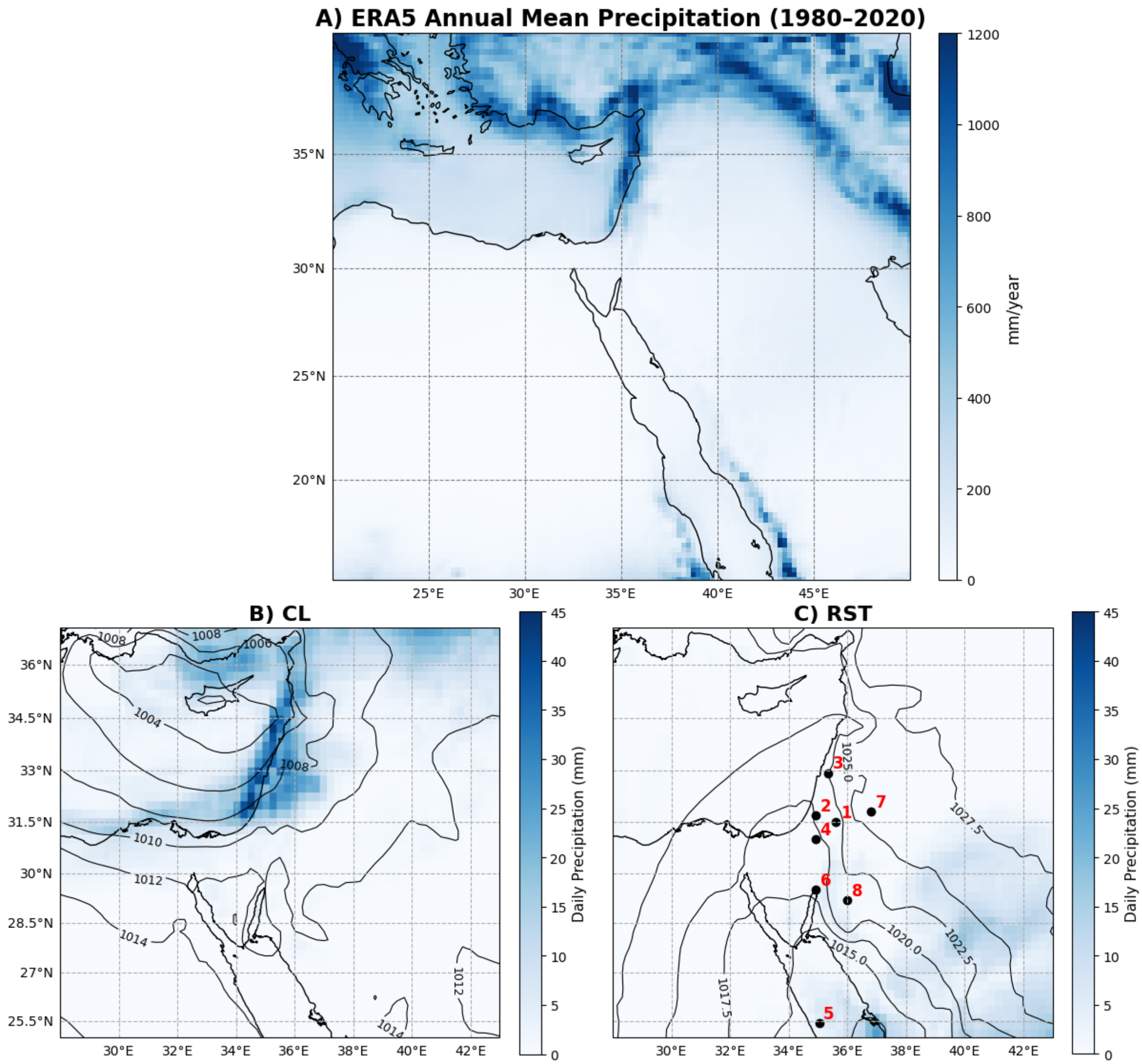

Figure 1. Average annual rainfall in the Mediterranean between 1980-2020 from ERA5 (A). Mean sea level pressure and precipitation maps of rain-bearing weather type examples in the Levant. Cyprus Low on 31 January 1992 (B). Red Sea Trough on 10 January 1992 (C). The location of geological archives for the LIG peak is in red: 1. Dead Sea (Torfstein et al., 2013, 2015; Kiro et al., 2020), 2. Soreq Cave (Bar-Matthews et al., 2003; Bar-Matthews, 2014), 3. Pequin Cave (Bar-Matthews et al., 2003; Bar-Matthews, 2014), 4. Negev Cave deposits (Vaks et al., 2003, 2006, 2007, 2010), 5. Red Sea core KL23 (Hartman et al., 2020; Palchan et al., 2018), 6. Fossilized corals (Lazar and Stein, 2011), 7. Azraq Oasis (Cordova et al., 2013), 8. Mudawara (Petit-Maire et al., 2010).

et al., 2013, 2015; Kiro et al., 2020; Kushnir et al., 2024) and the Red Sea (Hartman et al., 2020; Palchan et al., 2018), paleolakes in Jordan and Saudi Arabia (Petit-Maire et al., 2010; Rosenberg et al., 2013; Cordova et al., 2013), speleothem records from caves (Vaks et al., 2003, 2006, 2007, 2010; Fleitmann et al., 2003, 2011; Burns et al., 1998; McGarry et al., 2004; Bar-Matthews, 2014; Bar-Matthews et al., 2003), and coral studies (Lazar and Stein, 2011). The presence of cave deposits in the southern Levant dating back to MIS 5e (Vaks et al., 2007, 2003, 2006) suggests that their formation occurred under a hydrological regime significantly different from the present. Modern hydroclimatic conditions in the region do not support active speleothem growth, indicating that their development requires wetter and more favorable conditions than those currently prevailing.

Additional insights come from the Dead Sea Deep Drilling Project (DSDDP), which retrieved a sediment core capturing climatic conditions over the past 220,000 years (Torfstein et al., 2015; Neugebauer et al., 2014; Kiro et al., 2020). This core has revealed alternating aragonite and detrital laminae during the peak of the LIG, indicative of a wetter climate driven by increased freshwater inflow (Torfstein et al., 2015). In contrast, halite layers observed before and after this peak reflect the dominance of hyper-arid conditions in the long term. Several proxy-based studies have proposed potential drivers for the changes in hydroclimatic conditions observed at the LIG peak (Kiro et al., 2020; Palchan et al., 2018). These conditions have been attributed to significant changes in the frequency of rain-bearing weather types and a northward shift of tropical moisture sources toward the Levant (Kiro et al., 2020). For example, recently extracted sediment cores from the Red Sea have revealed increased local flooding events, enhanced soil transport, and elevated dust deposition from surrounding regions over time. This trend has been attributed to a higher frequency of "wet" Red Sea Trough (RST) or Tropical Plume (TP) weather patterns (Palchan et al., 2018; Hartman et al., 2020). Another likely contributing factor is the increased occurrence of Mediterranean cyclonic systems, which could have triggered intense rainfall and widespread flooding across the region (Waldmann et al., 2010; Vaks et al., 2010; Kutzbach et al., 2020; Tierney et al., 2022).

Analysis of the DSDDP core suggests an additional potential driver for the wetter conditions observed during the LIG peak. Located north of the Red Sea, current precipitation in the Dead Sea basin is primarily influenced by cyclonic systems originating from the Mediterranean (Goldreich, 2003; Hartman et al., 2020). However, studies of the DSDDP core indicate a secondary moisture source originating from the tropics, estimated to have contributed approximately 50% of precipitation, likely driven by a weakening of Mediterranean influence and a strengthening of tropical moisture transport (Kiro et al., 2020; Torfstein et al., 2015). This shift is attributed to the intensification of the African Summer Monsoon during the peak of the LIG (Kiro et al., 2020; Otto-Bliesner et al., 2021; Kutzbach et al., 2020; Orland et al., 2019). Building on these findings, proxy records from the hyper-arid regions south of the Dead Sea and around the Red Sea reveal wetter conditions and higher rainfall intensities during this period (Kiro et al., 2020; Palchan et al., 2018). Combined, these studies point to an enhanced influx of tropical sourced moisture consistent with the strengthened African Summer Monsoon as a key driver of the increased precipitation in the southern Levant at the peak of the LIG.

1.3 Model-based hydroclimate reconstruction of the LIG

Proxy records, which primarily capture coarse temporal and spatial scales in the late Quaternary and tend to be spatially limited, offer only a partial understanding of the mechanisms behind hydroclimatic variations in the Levant during the peak of the LIG

(Ludwig and Hochman, 2022; Otto-Bliesner et al., 2021; Kutzbach et al., 2020; Otto-Bliesner et al., 2013; Ludwig et al., 2019). To overcome these limitations, integrating proxy data with climate models provides a robust approach to exploring the drivers of paleoclimatic variability (Kiro et al., 2020; Kutzbach et al., 2020; Ludwig and Hochman, 2022; Otto-Bliesner et al., 2021; Consortium et al., 2017; Fischer et al., 2018; Jones et al., 2009). Although relatively few studies have used this approach for the Levant, climate model simulations have provided significant insights (Ludwig and Hochman, 2022; He et al., 2025). For example, increased precipitation in the Levant, particularly during summer, has been proposed based on an ensemble of PMIP4 models (Otto-Bliesner et al., 2021). This change has been further quantified using the CCSM3 model, reaching 0.5 mm per day (Kiro et al., 2020). In summary, findings from geochemical proxies and paleoclimate models have indicated relatively wetter conditions and changes in the source of precipitation in the southern Levant during the LIG peak. However, the specific mechanisms driving these changes and associated precipitation characteristics still need to be better understood.

This study aims to characterize the mechanisms underlying hydroclimatic changes during the LIG peak using PMIP4 models, a weather type classification, and dynamic-thermodynamic decomposition. The manuscript is organized as follows: Description of available reanalysis data and PMIP4 models (Sect. 2.1). The weather type classification method (Sect. 2.2). Moisture balance, i.e., Precipitation minus Evaporation and decomposition into its dynamic and thermodynamic components (Sect. 2.3). The Results are organized in three sections. Sect. 3.1 evaluates the PMIP4 model's ability to characterize the hydroclimate during the LIG peak. Sect. 3.2 provides insights into weather type characteristics during the LIG peak, focusing on the dominant rain-bearing weather types. Sect. 3.3 illustrates changes in moisture balance and the roles of dynamics and thermodynamics in these changes. Sect. 4 presents the main findings and interpretations of the model results regarding proxy data. Finally, Sect. 5 summarizes and concludes.

2 Data and methods

2.1 Data

We used data from nine General Circulation Models (GCM) contributing to the 4th Phase of the Paleo-climate Model Intercomparison Project (PMIP4; Kageyama et al. (2017)). PMIP4 is an ongoing international research initiative studying past climates using model simulations. It aims to improve our understanding of Earth's climate system by simulating and comparing various climate models from different periods in Earth's history. Most of our analysis was based on the Alfred Wagner Institute Earth System Model (AWI-ESM or AWI in short; Sidorenko et al. (2019)) and the 3rd generation of the European Community Earth System Model (EC-ESM or EC in short; Hazeleger et al. (2010)) available in daily temporal resolution and horizontal grid spacing of 2.5° ($\approx$ 280 km) and 1° ($\approx$ 111 km), respectively. The analysis was based on 40-year model runs for each period, including the LIG peak at 127 ka, the PI period (1850 CE), and the ERA5 reanalysis covering 1980–2020. Daily-resolution data were available only for the AWI-ESM and EC-Earth models, which were therefore used for the weather type classification described in Sect. 2.2. All available PMIP4 models were used at monthly resolution to evaluate the large-scale moisture balance (see Sect. 2.3), as this temporal resolution was adequate for the study objectives. The list of models is provided in Table 1.

For the weather type analysis in Sect. 2.2 we evaluated each model's ability to capture the precipitation values and weather type characteristics in the European Center for Medium-range Weather Forecast (ECMWF) reanalysis (ERA5) available at six hourly temporal resolution and a horizontal grid-spacing of 0.25° ($\approx$ 31 km) for 1980-2020 (Hersbach et al., 2020). To assess the statistical significance of differences in precipitation between the LIG and PI periods, we applied a non-parametric bootstrap resampling test (Tibshirani and Efron, 1993). In this approach, repeated random resampling with replacement was performed 1000 times within each period to generate a new empirical distribution of mean precipitation differences based on the original data. Statistical significance was determined at the 95% level, with differences considered significant when zero was outside the 95% confidence interval.

Model Name	Institution	Resolution	Reference
AWI-ESM-1-1-LR	Alfred Wegener Institute (AWI), Germany	250km	(Sidorenko et al., 2019; Shi et al., 2020)
FGOALS-g3	Chinese Academy of Sciences (CAS), China	250km	(He et al., 2020; Zheng et al., 2020)
ACCESS-ESM1-5	Australian Community Climate and Earth System Simulator + University of New South Wales, Australia	250km	(Ziehn et al., 2020; Yeung et al., 2021)
MIROC-ES2L	Research Institute for Global Change, Japan	500km	(Hajima et al., 2020; Ohgaito et al., 2020)
NorESM1-F	Norwegian Climate Centre (NCC), Norway	250km	(Guo et al., 2019)
NorESM2-LM	Norwegian Climate Centre (NCC), Norway	250km	(Seland et al., 2020; Zhang et al., 2019)
CESM2	National Center for Atmospheric Research (NCAR), USA	100km	(Danabasoglu et al., 2020)
NESM3	Nanjing University of Information Science and Technology (NUIST), China	250km	(Cao et al., 2018; Jian et al., 2019)
EC-Earth3-LR	European Community (EC), Europe	100km	(Hazeleger et al., 2010; Zhang et al., 2020b)

Table 1. List of nine PMIP4 models and their resolution, institutions and country. The results are described in Sect. 3.3.

2.2 Weather type classification

We employed the semi-objective synoptic classification algorithm originally developed by (Alpert et al., 2004b), which has been widely used in studies of the eastern Mediterranean climate (Alpert et al., 2004a, b; Hochman et al., 2018c; **?**; Ludwig and Hochman, 2022). The method is based on a reference archive of 426 days (1985 and winter 1991–1992), which five expert forecasters subjectively classified into 19 synoptic types. These types were later grouped into five primary weather types (daily scale): Persian Troughs, Highs, Sharav Lows, Red Sea Troughs, and Cyprus Lows. For each day, a feature vector is constructed from four near-surface atmospheric variables, geopotential height, temperature, and the zonal and meridional wind components, at 1000 hPa, averaged over a 5×5 grid covering the eastern Mediterranean domain (27.5–37.5° N, 30–40° E; Fig. 1B, C). Days from ERA5 and from the GCM simulations (AWI-ESM and EC-ESM; see Sect. 2.1) were then classified by assigning each to the expert-labeled reference day with the minimum Euclidean distance in this multidimensional space. This approach is considered semi-objective because it combines automated distance-based classification with limited expert verification, ensuring physical consistency of the resulting patterns. It has been shown to reproduce regional hydroclimatic variability with high fidelity. It provides physically interpretable weather types (Alpert et al., 2004a, b; Hochman et al., 2018c, b; Ludwig and Hochman, 2022), in contrast to unsupervised clustering methods that may produce clusters lacking clear synoptic meaning. We compared the average Euclidean distances among the three reference periods, the LIG peak, the PI period, and the

ERA5 reanalysis, to assess whether the weather type characteristics changed. The binomial test was then applied to compare the proportions of weather type frequencies between the LIG and PI periods at the 95% significance level.

2.3 Decomposing moisture balance into dynamic and thermodynamic components

The increase in wet conditions reflects a shift in water flux. The net water flux, defined as precipitation (P) minus evaporation (E) over a given surface, plays a fundamental role in the water cycle. While the globally averaged P minus E should theoretically balance to zero in current and future climates, assuming a closed system. However, regional variations can arise due to dynamic and thermodynamic processes influenced by climate change.

To investigate these processes, we applied a well-established decomposition framework following Seager et al. (2010), which separates the dynamic and thermodynamic components of the moisture balance between the LIG peak and the PI period.

In this framework, holding the humidity field constant isolates variations attributed to changes in the dynamic component, while modifications in the humidity field, with a fixed wind field, reflect adjustments in the thermodynamic component (Seager et al., 2010, 2019; Elbaum et al., 2022). This decomposition was applied to all nine PMIP4 models listed in Table 1 to ensure a robust assessment of the moisture-balance changes across the ensemble.

The precipitation-minus-evaporation balance is mathematically defined as follows:

$$\mathbf{P} - \mathbf{E} = -\frac{1}{g\rho_w} \nabla \cdot \sum_{k=1}^{k} \mathbf{u}_k \mathbf{q}_k dp_k \tag{1}$$

Where **g** is the acceleration of gravity, ρ_w is the density of water, **u** is the horizontal component of the wind, **q** is the specific humidity, **p** is the pressure, and κ is the vertical layers of the model. All variables are monthly averages (over-bars in Equation 2).

In Equation 2, the first term represents the large-scale, long-term mean moisture transport, computed using the monthly averages of wind ($\overline{\mathbf{u}_k}$) and specific humidity ($\overline{q}_k$). This term refers to persistent atmospheric circulation patterns, such as trade winds and monsoons, which are crucial in regulating regional and global moisture distribution.

The second term captures short-term variability driven by transient eddies ($\mathbf{u}_k^{'}$ and $q_k^{'}$), which represent atmospheric disturbances such as storms and cyclones. These fluctuations are key in moisture transport, particularly within mid-latitude storm tracks, contributing to episodic and intense precipitation events.

$$\overline{\mathbf{P}} - \overline{\mathbf{E}} = -\frac{1}{g\rho_w} \left[\nabla \cdot \left(\sum_{k=1}^{k} \overline{\overline{\mathbf{u}_k \mathbf{q}_k} dp_k} \right) + \nabla \cdot \left(\sum_{k=1}^{k} \overline{\overline{\mathbf{u}_k^{'} \mathbf{q}_k^{'}} dp_k} \right) \right] \tag{2}$$

In practice, we focused on the change (Δ) between the LIG peak and PI periods (Equation 3).

$$\Delta(\overline{P} - \overline{E}) \approx -\frac{1}{g\rho_w} \sum_{k=1}^{K} \Delta\overline{(\overline{\mathbf{u}}_k \cdot \nabla \overline{q}_k)} dp_k - \frac{1}{g\rho_w} \sum_{k=1}^{K} \Delta\overline{(\overline{q}_k \nabla \cdot \overline{\mathbf{u}}_k)} dp_k \tag{3}$$

The right-hand side of Equation 3 can be decomposed into three key components: dynamic, thermodynamic, and eddy variability.

- **Dynamic Component** – Represents changes in wind fields, capturing shifts in atmospheric circulation patterns that influence moisture transport (Equation 4).
- **Thermodynamic Component** – Reflects variations in the moisture content driven by temperature and humidity changes, affecting the atmospheric water's overall holding capacity (Equation 5).
- **Eddy Variability Component** – Derived from the second term in Equation 2, this component accounts for short-term fluctuations caused by transient eddies, such as storms and cyclones, which enhance episodic moisture transport (Equation 6).

$$\Delta \text{Dynamic} = -\frac{1}{g\rho_w}\sum_{k=1}^{K}\Delta\left(\overline{\mathbf{u}}_k\, dp_k\right)\cdot\nabla\overline{q}_{k,p_i} - \frac{1}{g\rho_w}\sum_{k=1}^{K}\overline{q}_{k,p_i}\Delta\left(\nabla\cdot\overline{\mathbf{u}}_k\, dp_k\right) \tag{4}$$

$$\Delta \text{Thermodynamic} = -\frac{1}{g\rho_w}\sum_{k=1}^{K}\overline{\mathbf{u}}_{k,p_i}\cdot\Delta\left(\nabla\overline{q}_k\, dp_k\right) - \frac{1}{g\rho_w}\sum_{k=1}^{K}\nabla\cdot\overline{\mathbf{u}}_{k,p_i}\Delta\left(\overline{q}_k\, dp_k\right) \tag{5}$$

$$\Delta \text{Eddys} = -\frac{1}{g\rho_w}\sum_{k=1}^{K}\Delta\left(\nabla\cdot\left(\mathbf{u}_k^{'}q_k^{'}\, dp_k\right)\right) \tag{6}$$

3 Results

3.1 Evaluating PMIP4 models concerning proxies and reanalysis

First, we evaluate the PMIP4 models to assess whether the simulated seasonal frequency of weather types corresponds to the observed climatological patterns with Cyprus Lows (CL) dominating in winter and Persian Troughs (PT) prevailing in summer, and to the precipitation seasonality inferred from proxy-based reconstructions (see Sect. 1.2, 1.3). Previous studies comparing precipitation between AWI-ESM and ERA5 reanalysis have indicated that AWI-ESM effectively captures the Levant's hydroclimate (Ludwig and Hochman, 2022). The two climate models diverge in representing seasonal precipitation differences between the LIG peak and PI periods (Fig. 2). Both models exhibit a comparable increase in winter precipitation relative to the PI period, with the most pronounced changes occurring in the northwestern Levant. During summer, the models differ significantly: AWI-ESM indicates increased precipitation, particularly in the southern Levant, aligned with evidence of intensified weathering near the Red Sea (Palchan et al., 2018), and transitions in Dead Sea sedimentation from salt to laminated silts (Kiro et al., 2020; Torfstein et al., 2015). However, EC-ESM shows a further southward change in summer precipitation. Autumn patterns also vary: AWI-ESM indicates drying in the northern Levant and increased precipitation in the south, whereas EC-ESM shows precipitation increases limited to the northern Mediterranean coasts, while the rest of the region remains relatively dry. In spring, both models show a slight increase in precipitation; the AWI-ESM model indicates an increase mainly in the northern Levant, while the EC-ESM model shows a more pronounced increase primarily in the southern Levant (Fig. 2).

The models exhibit distinct precipitation patterns. In AWI-ESM, autumn and summer precipitation is primarily concentrated in the southern regions (Fig. 2A, D), consistent with proxy evidence indicating higher rainfall intensity during the LIG compared to the PI and present periods, along with enhanced weathering in the Red Sea and Dead Sea areas, driven by tropical systems (Palchan et al., 2018; Kiro et al., 2020). In contrast, EC-ESM depicts minimal changes, with precipitation shifts occurring mainly in the northern part of the domain. (Fig. 2E, H).

We evaluated weather type frequencies to explore potential drivers of precipitation differences between the three periods. The y-axis in Fig. 3 represents the frequency of occurrence in percentages of each weather type, expressed as the percentage of days within each season. Both models effectively capture the seasonal-scale frequencies of weather types compared to ERA5 (Fig. 3A–H). We compared the frequency of weather types between the LIG and PI periods to identify potential differences in their seasonal occurrence patterns (Fig. 3). In autumn, both models show an increase in Red Sea Trough frequency during the LIG compared to the PI, though the signal is stronger in EC-ESM (Fig. 3A, E). During winter, the frequency of Cyprus Lows in AWI-ESM increases from about 40% of winter days in the PI to roughly 50% in the LIG, while EC-ESM shows no substantial changes (Fig. 3B, F). In spring, neither model displays statistically significant differences in weather type frequencies between the two periods (Fig. 3C, G). During summer, both models show no changes in known rain-bearing systems; however, the Persian Trough becomes more dominant in AWI-ESM, affecting over 90% of summer days during the LIG peak. In EC-ESM, Red Sea Trough frequencies increase in autumn, but neither model exhibits statistically significant weather type frequency changes between the LIG peak and PI periods. (Fig. 3D, H).

Determining the factors driving model differences is complex, but several key explanations emerge. AWI-ESM incorporates interactive vegetation, whereas EC-ESM relies on prescribed vegetation modules. Additionally, EC-ESM exhibits reduced winter ice extent during the LIG peak compared to the PI period (Kageyama et al., 2021), contributing to a larger positive temperature anomaly relative to other PMIP4 models, including AWI-ESM (Otto-Bliesner et al., 2021). Given that EC-ESM diverges from other models and proxy reconstructions (Zhang et al., 2020a), we prioritize AWI-ESM, which more reliably captures the Levant's hydroclimate during both the LIG and Last Glacial Maximum peaks (Ludwig and Hochman, 2022).

3.2 The hydroclimate during the LIG peak

Analysis of precipitation by weather type suggests a 17.3% increase in the daily average precipitation during Cyprus Low days in the AWI-ESM model compared to the PI period, with the most pronounced increase observed in the northern Levant, particularly over Turkey (Fig. 4A). Similarly, a quantitative analysis reveals a 23.3% increase in daily mean precipitation during Red Sea Trough days, as determined by a direct comparison of mean daily precipitation between the two periods. While the

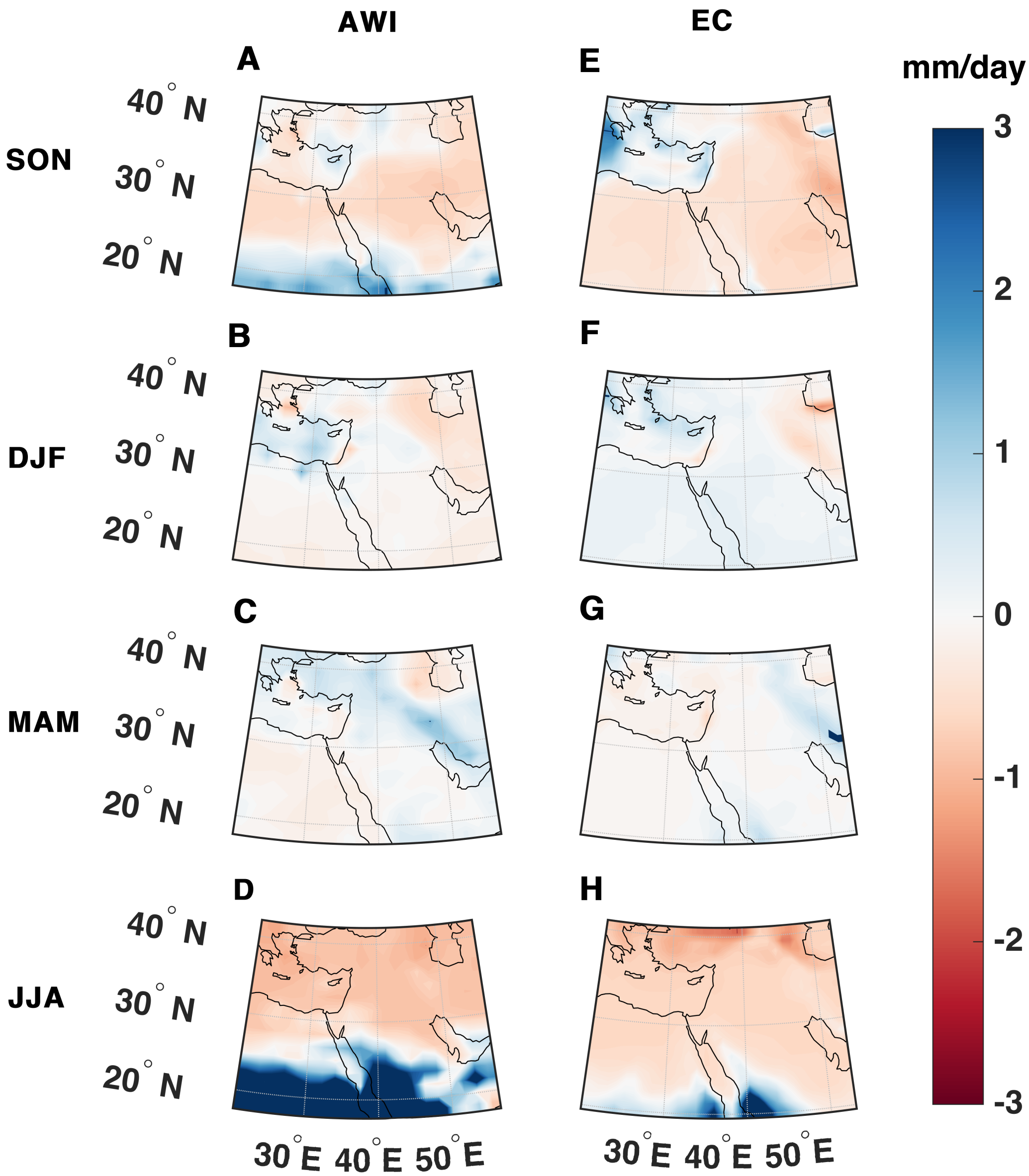

Figure 2. The difference between LIG - PI in precipitation [mm/d]. For every season: Autumn- September, October, November [SON - A, E]. Winter- December, January, February [DJF - B, F]. Spring- March, April, May [MAM - C, G]. Summer- June, July, August [JJA - D, H]. In two models, AWI-ESM [AWI; A-D] and EC-ESM [EC; E-H]. Colored regions denote statistically significant changes at the 95% level as determined by a bootstrap test.

figures do not explicitly display these computed values, Figure 4B highlights the spatial distribution of precipitation changes, illustrating areas where the daily average precipitation during Red Sea Trough days increased, particularly around the Red Sea, as well as in other parts of the Levant. In contrast, during the Cyprus Low days, the increase in precipitation is mainly confined to the northern Levant. This increase is most pronounced in autumn, winter, and spring, while summer sees a minor impact due to the relatively low frequency of Red Sea Trough occurrences during this season (Fig. 3).

High-percentile precipitation events (90th percentile of precipitation days) exhibit even greater differences between the LIG peak and the PI period, with significantly higher precipitation intensities recorded during Cyprus Low (Fig. 4C) and Red Sea Trough (Fig. 4D) days. Notably, this increase is most evident in the northern Levant, where the frequency and intensity of high-percentile precipitation events have risen. In contrast, while localized increases are observed in the southern Levant, high-percentile precipitation values have generally remained unchanged or even declined in some areas. We note that the analysis was conducted annually, considering all Cyprus Low or Red Sea Trough days. As shown in Fig. 3, these systems are predominantly active during autumn, winter, and spring, with a limited presence in summer.

At first glance, Figure 4 may appear to contrast with proxy-based findings described in the Introduction, which indicates a general increase in average and high-percentile precipitation events across the Mediterranean region. However, a closer examination reveals a more nuanced pattern. The data show that this increase is primarily associated with Cyprus Lows, a characteristic Mediterranean weather system. Additionally, precipitation linked to Red Sea Troughs increases, but these systems can draw moisture from either the Mediterranean, as in the Cyprus Lows, or from southern moisture sources (Tsvieli and Zangvil, 2007; Hochman et al., 2023). Proxy-based studies have frequently highlighted increased precipitation from southern sources rather than Mediterranean ones. This suggests that the observed precipitation characteristics on Red Sea Trough days may reflect a shift in moisture sources, aligning with proxy evidence of enhanced contributions from the south (Palchan et al., 2018; Kiro et al., 2020).

To further characterize precipitation variability during the LIG peak, we examine transitions between weather types using the weather type transition probability matrix (Table 2). This matrix quantifies the likelihood of one weather type transitioning to another the following day, enabling comparisons between the LIG peak and the preindustrial period across seasons and on an annual scale. Our analysis reveals that Cyprus Lows exhibited 6.4% greater persistence in winter during the LIG peak (Table 2B) and a 4.8% increase annually (Table 2E). Meanwhile, Red Sea Troughs showed the largest increase in persistence during autumn at 2.2% (Table 2A), although the annual change was minimal at 0.2%.

3.3 Identifying the drivers of hydroclimate changes in the LIG peak

Analyzing the moisture balance, i.e., the difference between precipitation and evaporation ($\Delta P - E$), provides a deeper insight into the hydroclimatic differences between the LIG peak and the PI period. During autumn, the moisture balance shows a moderate increase, mainly over Northeast Africa (Egypt) and parts of the southern Levant (Fig. 5). In winter, the changes are statistically significant but relatively small in magnitude compared to other seasons, with localized decreases over Israel and nearby regions. In spring, the entire Levant experiences an overall increase in the moisture balance, indicating enhanced water availability across the region. During summer, a marked increase is observed, particularly over the southern Levant and the northern Red Sea, reflecting higher moisture availability relative to the PI period (Fig. 5).

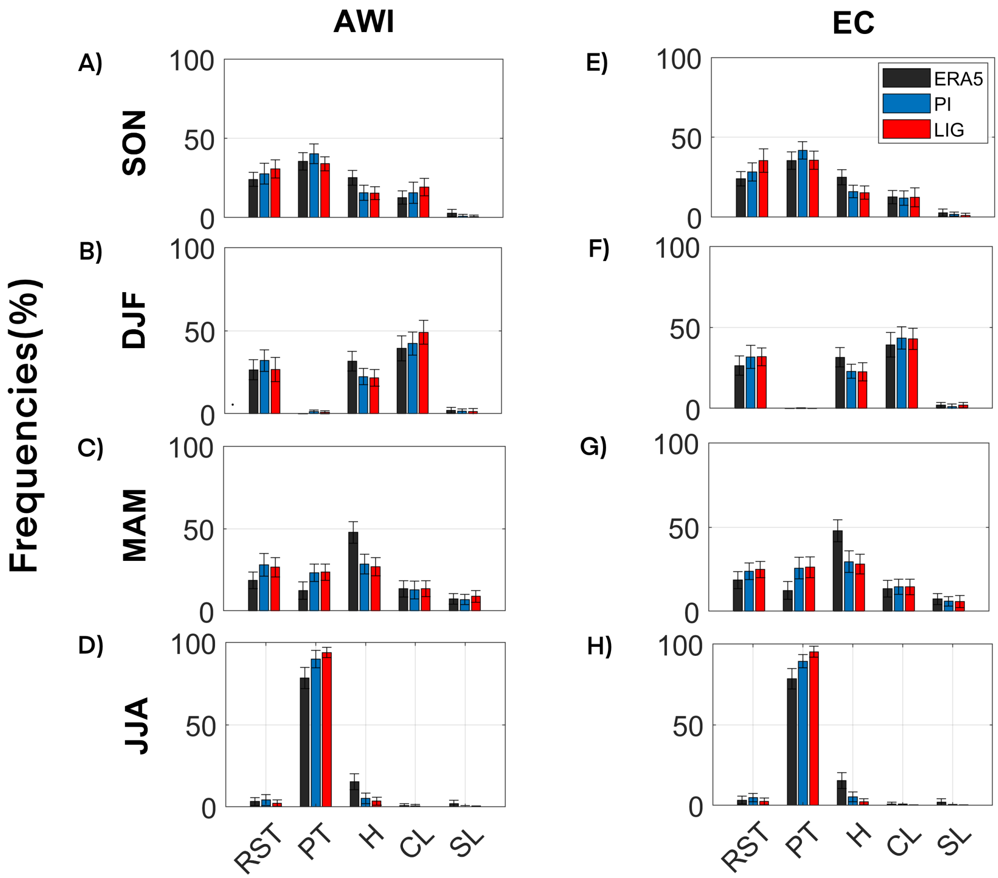

Figure 3. The seasonal frequencies of weather types in the Levant. Autumn- September, October, November [SON - A, E]. Winter - December, January, February [DJF - B, F]. Spring - March, April, May [MAM - C, G]. Summer - June, July, August [JJA - D, H]. For three time periods: ERA5 reanalysis [ERA5], LIG peak, and PI. The weather types are Red Sea Trough [RST], Persian Trough [PT], High-pressure systems [H], Cyprus Low [CL] and Sharav Low [SL]. Two models were considered: the AWI-ESM [AWI; A-D] and the EC-ESM [EC; E-H].

When decomposing these changes into dynamic and thermodynamic components, we find that the summer increase in moisture balance is primarily driven by the thermodynamic component, indicating higher moisture availability in the Levant (Fig. 6J-L). This increase is consistent with previous studies (Otto-Bliesner et al., 2021) on the LIG peak, highlighting that most of the warming occurred during summer. Across different PMIP4 models presented in Table 1, summer temperatures in the Levant rose by more than 4°C to 7°C consistent with previous studies (Otto-Bliesner et al., 2013, 2021). In contrast, winter temperatures exhibited a cooling trend (Otto-Bliesner et al., 2021, 2013), likely contributing to a reduction in the moisture balance (Fig. 6D-F). This seasonal contrast highlights the crucial role of the thermodynamic component in summer, as warmer air can hold more water vapor, thereby increasing its capacity to transport moisture into the Levant.

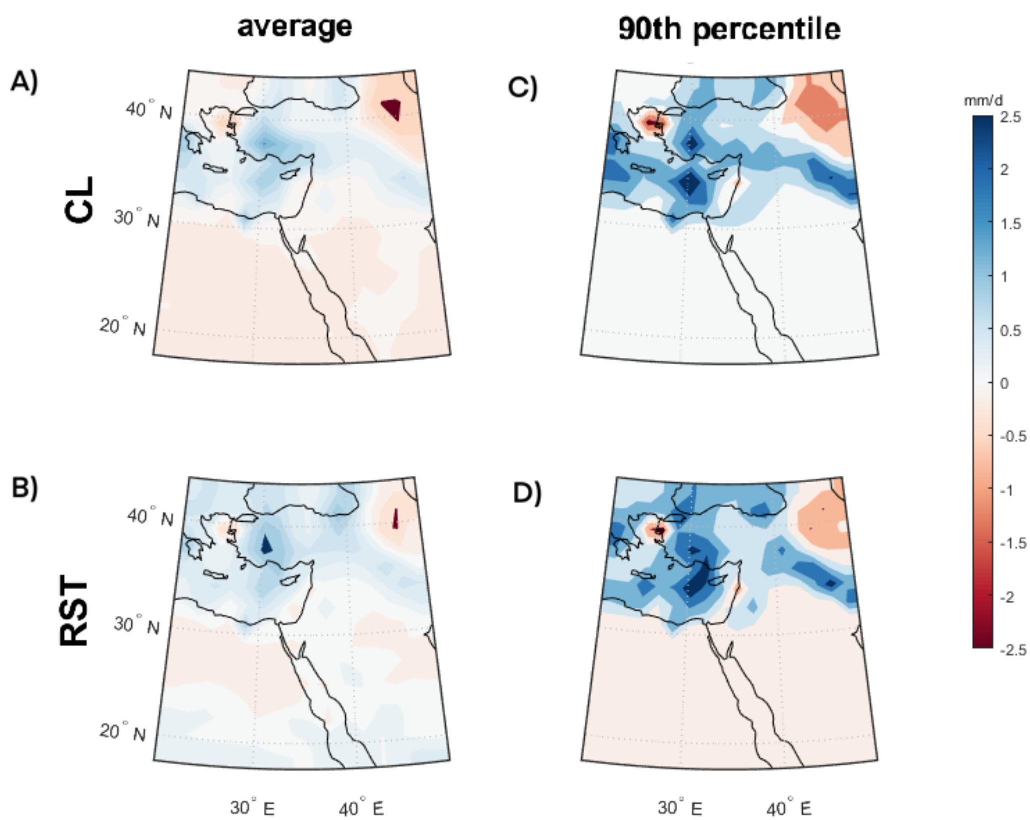

Figure 4. Differences in average and 90th percentile of precipitation [mm/d] for Red Sea Trough [RST] and Cyprus Low [CL] between the LIG peak and PI periods. Colored regions denote statistically significant changes at the 95% level as determined by a bootstrap test.

The dynamic component remains largely unchanged and shows a decline in some regions. This decline suggests that large-scale circulation patterns played a lesser role in moisture transport during this period. The reduced influence of the dynamic component is particularly pronounced in summer and autumn, reinforcing the notion that thermodynamic processes were the dominant drivers of moisture balance during these seasons. In autumn and winter, the dynamic component contributes less to the overall moisture balance. However, in the spring, it exhibits a marked increase in the Levant, accounting for much of the seasonal rise in moisture availability (Fig. 6B, E). The position and strength of the jet stream were also analyzed, revealing no significant changes (not shown), further supporting the limited role of large-scale circulation shifts in driving variations in moisture balance (Kutzbach et al., 2020; Kushnir et al., 2024).

These seasonal variations highlight the complex interplay of atmospheric processes, emphasizing a shifting balance between thermodynamic and dynamic factors throughout the year. The results are based on the multi-model mean of nine PMIP4 simulations, ensuring robustness and consistency across different climate models (see Table 1).

A

		AWI SON LIG-PI				
		probability for the next day				
	system	RST	PT	H	CL	SL
today	RST	2.2	-2.9	-2.0	3.5	-0.7
	PT	-0.4	-0.7	0.3	0.5	0.2
	H	0.3	-2.4	0.4	2.2	-0.7
	CL	3.2	-3.0	-1.6	1.5	-0.1
	SL	-8.3	5.2	13.5	-17.7	7.3

B

		AWI MAM LIG-PI				
		probability for the next day				
	system	RST	PT	H	CL	SL
today	RST	1.6	-4.2	2.1	0.4	-0.1
	PT	-2.6	5.0	-5.4	0.6	2.3
	H	-1.3	0.9	-2.5	1.3	1.7
	CL	-1.4	-1.6	-0.2	1.8	1.5
	SL	-3.1	1.9	-1.0	-1.4	3.9

C

		AWI DJF LIG-PI				
		probability for the next day				
	system	RST	PT	H	CL	SL
today	RST	-3.8	-0.3	-0.2	4.2	0.1
	PT	-8.3	0.0	-15.1	28.1	-4.1
	H	-4.0	-0.3	2.1	1.5	0.8
	CL	-4.5	-0.3	-0.5	6.4	-1.1
	SL	-0.1	-1.1	-6.9	4.2	4.0

D

		AWI JJA LIG-PI				
		probability for the next day				
	system	RST	PT	H	CL	SL
today	RST	-17.3	22.4	-4.4	0.0	-0.7
	PT	-1.0	1.9	-0.8	-0.2	0.0
	H	-0.1	6.6	-4.4	-1.0	-0.8
	CL	0.0	50.0	-11.1	-38.9	0.0
	SL	16.7	45.8	-62.5	0.0	0.0

E

		LIG-PI				
		probability for the next day				
	system	RST	PT	H	CL	SL
today	RST	0.2	-2.1	-0.3	2.4	-0.2
	PT	-1.4	2.6	-1.4	-0.1	0.4
	H	-1.3	-1.3	-0.3	2.2	0.7
	CL	-2.0	-1.4	-1.0	4.8	-0.4
	SL	-2.3	1.8	-2.5	-2.4	5.4

Table 2. Weather type transition probability matrix. The difference between the LIG peak and PI periods. The weather types are Red Sea Trough [RST], Persian Trough [PT], High [H], Cyprus Low [CL], and Sharav Low [SL]. For every season: Autumn [SON - A], Winter [DJF - B], Spring [MAM - C], Summer [JJA - D], and annual [E]. Statistically significant differences are marked with an underline using a binomial test at the 95% significance level.

4 Discussion

Proxy records indicate that the LIG was generally hyper-arid in the Levant; however, during its peak (MIS 5e), episodic wet phases occurred, driven by moisture intrusions from southern sources (Torfstein, 2019, 2024). Some studies link these shifts to a northward expansion of the African Summer Monsoon (Kiro et al., 2020). However, we suggest that Red Sea Trough intensification better explains the observed changes, as it primarily affects the Levant in autumn and winter rather than summer. Thus, increased northern Levant precipitation likely reflects enhanced autumn and winter rainfall rather than wetter summers.

In contrast, regions near the Red Sea are influenced by the African Summer Monsoon and Tropical Plumes, which drive summer rainfall in East Africa and increase Nile River flow (Bar-Matthews et al., 2000; Rohling et al., 2002). The Red Sea Trough, however, remains active during transitional seasons and winter (Tsvieli and Zangvil, 2005, 2007; Ziv et al., 2022). Both systems transport moisture from the south, but the Red Sea Trough exerts a broader climatic impact over the Levant. Indeed, there is a 23% increase in average precipitation during Red Sea Trough days. This increased southern precipitation

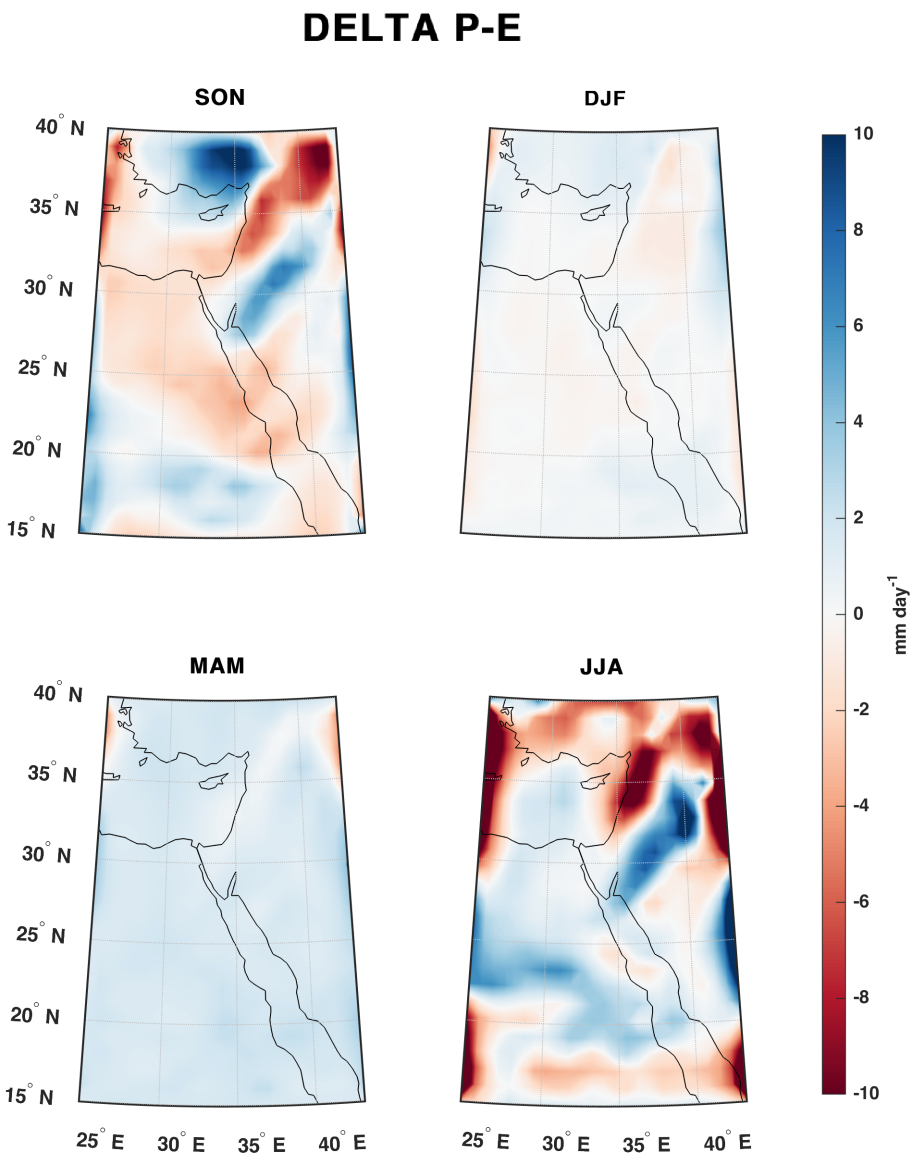

Figure 5. Delta Precipitation - Evaporation $\Delta P - E$ [mm/d] for the LIG peak compared to the PI period. For every season: Autumn- [SON - A], Winter [DJF - B], Spring [MAM - C], and Summer [JJA - D]. Colored regions denote statistically significant changes at the 95% level as determined by a bootstrap test.

during MIS5e likely resulted from intensified Red Sea Trough events, contributing to a more substantial climatic effect across the region.

Proxy records from central Israel do not strongly support greater summer rainfall but instead suggest higher precipitation intensity, likely due to a stronger Red Sea Trough, active from October to May. Climate models confirm this pattern, showing an increase in daily rainfall linked to the Red Sea Trough (Fig. 4), while summer rainfall increases remained localized along the Red Sea coast (Otto-Bliesner et al., 2021; Kutzbach et al., 2020).

5 Summary and Conclusions

This study examines the hydroclimate conditions in the Levant during the LIG peak, focusing on the characteristics of weather types and the drivers of moisture balance. Drawing on previous proxy-based reconstructions (Torfstein et al., 2015; Torfstein, 2019; Kiro et al., 2020) and climate model simulations (Otto-Bliesner et al., 2021; Shi et al., 2020) from the 4th phase of the Paleo-climate Model Inter-comparison Project (PMIP4), we analyze seasonal moisture balance patterns, particularly in the southern Levant. Our results reveal that thermodynamic changes influenced moisture availability during the LIG peak, increasing atmospheric moisture capacity, especially in summer and autumn. Decomposing the moisture balance into thermodynamic and dynamic components shows that the thermodynamic contribution was the dominant factor in shaping seasonal moisture conditions. In contrast, changes in the dynamic component were minimal. The study also highlights the role of synoptic-scale weather types, such as Cyprus Lows and Red Sea Troughs, in shaping regional moisture patterns. While an increase in moisture availability is observed during the LIG peak, only small changes are detected in the frequency of these weather types. The study highlights the importance of integrating climate models with proxy data to enhance our understanding of past climate variability and its implications for future climate projections. Despite advancements, we acknowledge limitations in model resolution and temporal coverage, suggesting that further investigations are necessary to refine our knowledge of regional hydroclimate processes (Hochman et al., 2018a). Ultimately, this study provides valuable insights into the dynamics of moisture balance during the LIG and aids in the development of future climate scenarios, considering both natural variability and anthropogenic influences.

Data availability. All data used in this study is publicly available. We acknowledge the climate modeling groups for producing and providing access to their model output, as well as the Earth System Grid Federation (ESGF) for archiving and facilitating data access. The results and conclusions presented here are based on two key datasets: the 5th generation of the European Centre for Medium-Range Weather Forecasts (ECMWF) ERA5 reanalysis dataset www.ecmwf.int/en/forecasts/datasets/reanalysis-datasets/era5 and multiple simulations from the Paleoclimate Model Intercomparison Project Phase 4 (PMIP4). We thank the multiple funding agencies that support PMIP and ESGF. All PMIP4 data analyzed in this study are available through the ESGF at https:https://esgf-node.llnl.gov/projects/esgf-llnl

Author contributions. The following is a detailed breakdown of each author's contributions to the manuscript. **EB** : Conceptualization; Methodology; Formal Analysis; Software; Validation; Data Curation; Writing – Original Draft; Visualization. **AT**: Supervision; Conceptu-

alization; Methodology; Writing – Review & Editing; Funding Acquisition. **AH** : Supervision; Conceptualization; Methodology; writing – Review & Editing; Funding Acquisition. **RY**: Software; Validation.

Competing interests. The authors have no relevant financial or non-financial interests to disclose.

Acknowledgements. The Israel Science Foundation (grant 978/23), the Pazy Foundation (grant 434), the Federal Ministry of Education and Research (BMBF), Germany and the Ministry of Innovation Science and Technology of Israel within the GRaCCE project, the COST Actions CA19109 and CA22162, 'MedCyclones' and 'FutureMed' supported by COST (European Cooperation in Science and Technology), the Nuclear Research Center of the Negev, and the Planning and Budgeting Committee of the Israeli Council for Higher Education under the 'Med World' Consortium provide support for the contribution of AH, EB and RY. The authors acknowledge using Grammarly (https://www.grammarly.com) and ChatGPT 5.2 for English editing purposes, and the editor and two anonymous reviewers for providing constructive feedback on an earlier version of the manuscript.

References

Alpert, P., Osetinsky, I., Ziv, B., and Shafir, H.: A new seasons definition based on classified daily synoptic systems: an example for the eastern Mediterranean, International Journal of Climatology: A Journal of the Royal Meteorological Society, 24, 1013–1021, https://doi.org/https://doi.org/10.1002/joc.1037, 2004a.

Alpert, P., Osetinsky, I., Ziv, B., and Shafir, H.: Semi-objective classification for daily synoptic systems: Application to the eastern Mediterranean climate change, International Journal of Climatology: A Journal of the Royal Meteorological Society, 24, 1001–1011, https://doi.org/https://doi.org/10.1002/joc.1036, 2004b.

Armon, M., Morin, E., and Enzel, Y.: Overview of modern atmospheric patterns controlling rainfall and floods into the Dead Sea: Implications for the lake's sedimentology and paleohydrology, Quaternary Science Reviews, 216, 58–73, https://doi.org/https://doi.org/10.1016/j.quascirev.2019.06.005, 2019.

Armon, M., Marra, F., Enzel, Y., Rostkier-Edelstein, D., Garfinkel, C. I., Adam, O., Dayan, U., and Morin, E.: Reduced rainfall in future heavy precipitation events related to contracted rain area despite increased rain rate, Earth's Future, 10, e2021EF002 397, https://doi.org/https://doi.org/10.1002/essoar.10507881.2, 2022.

Bar-Matthews, M.: History of water in the Middle East and North Africa, https://doi.org/https://doi.org/10.1163/1872-5309_ewic_ewiccom_0049, 2014.

Bar-Matthews, M., Ayalon, A., and Kaufman, A.: Timing and hydrological conditions of Sapropel events in the Eastern Mediterranean, as evident from speleothems, Soreq cave, Israel, Chemical Geology, 169, 145–156, https://doi.org/https://doi.org/10.1016/s0009-2541(99)00232-6, 2000.

Bar-Matthews, M., Ayalon, A., Gilmour, M., Matthews, A., and Hawkesworth, C. J.: Sea–land oxygen isotopic relationships from planktonic foraminifera and speleothems in the Eastern Mediterranean region and their implication for paleorainfall during interglacial intervals, Geochimica et cosmochimica acta, 67, 3181–3199, https://doi.org/https://doi.org/10.1016/s0016-7037(02)01031-1, 2003.

Bar-Yosef, O.: On the nature of transitions: the Middle to Upper Palaeolithic and the Neolithic Revolution, Cambridge Archaeological Journal, 8, 141–163, https://doi.org/https://doi.org/10.1017/s0959774300001815, 1998.

Bookman, R., Bartov, Y., Enzel, Y., and Stein, M.: Quaternary lake levels in the Dead Sea basin: two centuries of research, New Frontiers in Dead Sea Paleoenvironmental Research, https://doi.org/https://doi.org/10.1130/2006.2401(10), 2006.

Burns, S. J., Matter, A., Frank, N., and Mangini, A.: Speleothem-based paleoclimate record from northern Oman, Geology, 26, 499–502, https://doi.org/https://doi.org/10.1130/0091-7613(1998)026<0499:sbprfn>2.3.co;2, 1998.

Cao, J., Wang, B., Yang, Y.-M., Ma, L., Li, J., Sun, B., Bao, Y., He, J., Zhou, X., and Wu, L.: The NUIST Earth System Model (NESM) version 3: description and preliminary evaluation, Geoscientific Model Development, 11, 2975–2993, https://doi.org/https://doi.org/10.5194/gmd-2017-206, 2018.

Consortium, P. H. et al.: Comparing proxy and model estimates of hydroclimate variability and change over the Common Era, Climate of the Past, 13, 1851–1900, https://doi.org/https://doi.org/10.5194/cp-2017-37, 2017.

Cordova, C. E., Nowell, A., Bisson, M., Ames, C. J., Pokines, J., Chang, M., and al Nahar, M.: Interglacial and glacial desert refugia and the Middle Paleolithic of the Azraq Oasis, Jordan, Quaternary International, 300, 94–110, https://doi.org/https://doi.org/10.1016/j.quaint.2012.09.019, 2013.

Danabasoglu, G., Lamarque, J.-F., Bacmeister, J., Bailey, D., DuVivier, A., Edwards, J., Emmons, L., Fasullo, J., Garcia, R., Gettelman, A., et al.: The community earth system model version 2 (CESM2), Journal of Advances in Modeling Earth Systems, 12, e2019MS001 916, https://doi.org/https://doi.org/10.1029/2019ms001916, 2020.

Derricourt, R.: Getting "Out of Africa": sea crossings, land crossings and culture in the hominin migrations, Journal of world prehistory, 19, 119–132, https://doi.org/https://doi.org/10.1007/s10963-006-9002-z, 2005.

Dutton, A. and Lambeck, K.: Ice volume and sea level during the last interglacial, science, 337, 216–219, https://doi.org/https://doi.org/10.1126/science.1205749, 2012.

Elbaum, E., Garfinkel, C. I., Adam, O., Morin, E., Rostkier-Edelstein, D., and Dayan, U.: Uncertainty in projected changes in precipitation minus evaporation: Dominant role of dynamic circulation changes and weak role for thermodynamic changes, Geophysical Research Letters, 49, e2022GL097 725, https://doi.org/https://doi.org/10.5194/egusphere-egu22-1381, 2022.

Enzel, Y. and Bar-Yosef, O.: Quaternary of the Levant: environments, climate change, and humans, Cambridge University Press, https://doi.org/https://doi.org/10.4000/paleorient.616, 2017.

Fischer, H., Meissner, K. J., Mix, A. C., Abram, N. J., Austermann, J., Brovkin, V., Capron, E., Colombaroli, D., Daniau, A.-L., Dyez, K. A., et al.: Palaeoclimate constraints on the impact of 2 C anthropogenic warming and beyond, Nature geoscience, 11, 474–485, https://doi.org/https://doi.org/10.1038/s41561-018-0146-0, 2018.

Fleitmann, D., Burns, S. J., Neff, U., Mangini, A., and Matter, A.: Changing moisture sources over the last 330,000 years in Northern Oman from fluid-inclusion evidence in speleothems, Quaternary Research, 60, 223–232, https://doi.org/https://doi.org/10.1016/s0033-5894(03)00086-3, 2003.

Fleitmann, D., Burns, S. J., Pekala, M., Mangini, A., Al-Subbary, A., Al-Aowah, M., Kramers, J., and Matter, A.: Holocene and Pleistocene pluvial periods in Yemen, southern Arabia, Quaternary Science Reviews, 30, 783–787, https://doi.org/https://doi.org/10.1016/j.quascirev.2011.01.004, 2011.

Goldreich, Y.: The climate of Israel: observation, research, and application, Springer, https://doi.org/https://doi.org/10.1191/0309133303pp392xx, 2003.

Govin, A., Capron, É., Tzedakis, P., Verheyden, S., Ghaleb, B., Hillaire-Marcel, C., St-Onge, G., Stoner, J. S., Bassinot, F., Bazin, L., et al.: Sequence of events from the onset to the demise of the Last Interglacial: Evaluating strengths and limitations of chronologies used in climatic archives, Quaternary Science Reviews, 129, 1–36, https://doi.org/https://doi.org/10.1016/j.quascirev.2015.09.018, 2015.

Guo, C., Bentsen, M., Bethke, I., Ilicak, M., Tjiputra, J., Toniazzo, T., Schwinger, J., and Otterå, O. H.: Description and evaluation of NorESM1-F: A fast version of the Norwegian Earth System Model (NorESM), Geoscientific Model Development, 12, 343–362, https://doi.org/https://doi.org/10.5194/gmd-12-343-2019, 2019.

Hajima, T., Watanabe, M., Yamamoto, A., Tatebe, H., Noguchi, M. A., Abe, M., Ohgaito, R., Ito, A., Yamazaki, D., Okajima, H., et al.: Development of the MIROC-ES2L Earth system model and the evaluation of biogeochemical processes and feedbacks, Geoscientific Model Development, 13, 2197–2244, https://doi.org/https://doi.org/10.5194/gmd-13-2197-2020, 2020.

Hartman, A., Torfstein, A., and Almogi-Labin, A.: Climate swings in the northern Red Sea over the last 150,000 years from εNd and Mg/Ca of marine sediments, Quaternary Science Reviews, 231, 106 205, https://doi.org/https://doi.org/10.1016/j.quascirev.2020.106205, 2020.

Hazeleger, W., Severijns, C., Semmler, T., Ştefănescu, S., Yang, S., Wang, X., Wyser, K., Dutra, E., Baldasano, J. M., Bintanja, R., et al.: EC-Earth: a seamless earth-system prediction approach in action, Bulletin of the American Meteorological Society, 91, 1357–1364, https://doi.org/https://doi.org/10.1088/1755-1307/6/5/052002, 2010.

He, B., Liu, Y., Wu, G., Bao, Q., Zhou, T., Wu, X., Wang, L., Li, J., Wang, X., Li, J., et al.: CAS FGOALS-f3-L model datasets for CMIP6 GMMIP Tier-1 and Tier-3 experiments, Advances in Atmospheric Sciences, 37, 18–28, https://doi.org/https://doi.org/10.1007/s00376-019-9085-y, 2020.

He, L., Biasutti, M., and Kushnir, Y.: Enhanced Mediterranean Wetting in Response to Cold Indian Ocean SST during the Last Interglacial, Journal of Climate, p. e250157, https://doi.org/https://doi.org/10.1175/JCLI-D-25-0157.1, 2025.

Hersbach, H., Bell, B., Berrisford, P., Hirahara, S., Horányi, A., Muñoz-Sabater, J., Nicolas, J., Peubey, C., Radu, R., Schepers, D., et al.: The ERA5 global reanalysis, QJR Meteorolog. Soc., 146, 1999–2049, https://doi.org/https://doi.org/10.1002/qj.3803, 2020.

Hochman, A., Bucchignani, E., Gershtein, G., Krichak, S. O., Alpert, P., Levi, Y., Yosef, Y., Carmona, Y., Breitgand, J., Mercogliano, P., et al.: Evaluation of regional COSMO-CLM climate simulations over the Eastern Mediterranean for the period 1979–2011, International Journal of Climatology, 38, 1161–1176, https://doi.org/https://doi.org/10.1002/joc.5232, 2018a.

Hochman, A., Harpaz, T., Saaroni, H., and Alpert, P.: The seasons' length in 21st century CMIP5 projections over the eastern Mediterranean, International Journal of Climatology, 38, 2627–2637, https://doi.org/https://doi.org/10.1002/joc.5448, 2018b.

Hochman, A., Harpaz, T., Saaroni, H., and Alpert, P.: Synoptic classification in 21st century CMIP5 predictions over the Eastern Mediterranean with focus on cyclones, International Journal of Climatology, 38, 1476–1483, https://doi.org/https://doi.org/10.1002/joc.5260, 2018c.

Hochman, A., Mercogliano, P., Alpert, P., Saaroni, H., and Bucchignani, E.: High-resolution projection of climate change and extremity over Israel using COSMO-CLM, International Journal of Climatology, 38, 5095–5106, https://doi.org/https://doi.org/10.1002/joc.5714, 2018d.

Hochman, A., Rostkier-Edelstein, D., Kunin, P., and Pinto, J. G.: Changes in the characteristics of 'wet'and 'dry'Red Sea Trough over the Eastern Mediterranean in CMIP5 climate projections, Theoretical and Applied Climatology, 143, 781–794, https://doi.org/https://doi.org/10.1007/s00704-020-03449-0, 2021.

Hochman, A., Plotnik, T., Marra, F., Shehter, E.-R., Raveh-Rubin, S., and Magaritz-Ronen, L.: The sources of extreme precipitation predictability; the case of the 'Wet' Red Sea Trough, Weather and Climate Extremes, 40, 100 564, https://doi.org/https://doi.org/10.1016/j.wace.2023.100564, 2023.

Jian, C., Li-Bin, M., Juan, L., WANG, B., and Bo, W.: Introduction of NUIST-ESM model and its CMIP6 activities, Advances in Climate Change Research, 15, 566, https://doi.org/10.12006/j.issn.1673-1719.2019.064, 2019.

Jones, P. D., Briffa, K. R., Osborn, T., Lough, J. M., van Ommen, T. D., Vinther, B. M., Luterbacher, J., Wahl, E., Zwiers, F., Mann, M. E., et al.: High-resolution palaeoclimatology of the last millennium: a review of current status and future prospects, The Holocene, 19, 3–49, https://doi.org/https://doi.org/10.1177/0959683608098952, 2009.

Jouzel, J., Masson-Delmotte, V., Cattani, O., Dreyfus, G., Falourd, S., Hoffmann, G., Minster, B., Nouet, J., Barnola, J.-M., Chappellaz, J., et al.: Orbital and millennial Antarctic climate variability over the past 800,000 years, science, 317, 793–796, https://doi.org/https://doi.org/10.1126/science.1141038, 2007.

Kageyama, M., Albani, S., Braconnot, P., Harrison, S. P., Hopcroft, P. O., Ivanovic, R. F., Lambert, F., Marti, O., Peltier, W. R., Peterschmitt, J.-Y., et al.: The PMIP4 contribution to CMIP6–Part 4: Scientific objectives and experimental design of the PMIP4-CMIP6 Last Glacial Maximum experiments and PMIP4 sensitivity experiments, Geoscientific Model Development, 10, 4035–4055, https://doi.org/https://doi.org/10.5194/gmd-2017-18, 2017.

Kageyama, M., Sime, L. C., Sicard, M., Guarino, M.-V., de Vernal, A., Stein, R., Schroeder, D., Malmierca-Vallet, I., Abe-Ouchi, A., Bitz, C., et al.: A multi-model CMIP6-PMIP4 study of Arctic sea ice at 127 ka: sea ice data compilation and model differences, Climate of the Past, 17, 37–62, https://doi.org/https://doi.org/10.5194/cp-17-37-2021, 2021.

Kahana, R., Ziv, B., Enzel, Y., and Dayan, U.: Synoptic climatology of major floods in the Negev Desert, Israel, International Journal of Climatology, 22, 867–882, https://doi.org/https://doi.org/10.1002/joc.766, 2002.

Kiro, Y., Goldstein, S. L., Kushnir, Y., Olson, J. M., Bolge, L., Lazar, B., and Stein, M.: Droughts, flooding events, and shifts in water sources and seasonality characterize last interglacial Levant climate, Quaternary Science Reviews, 248, 106 546, https://doi.org/https://doi.org/10.1016/j.quascirev.2020.106546, 2020.

Kushnir, Y., Stein, M., Biasutti, M., Kiro, Y., Goldsmith, Y., and Goldstein, S. L.: Paleo aridity in the Levant driven by a strong North Atlantic latitudinal surface temperature gradient and present-day relevance, Proceedings of the National Academy of Sciences, 121, e2407166 121, https://doi.org/https://doi.org/10.1073/pnas.2407166121, 2024.

Kutzbach, J. E., Guan, J., He, F., Cohen, A. S., Orland, I. J., and Chen, G.: INAUGURAL ARTICLE by a Recently Elected Academy Member: African climate response to orbital and glacial forcing in 140,000-y simulation with implications for early modern human environments, Proceedings of the National Academy of Sciences of the United States of America, 117, 2255, https://doi.org/https://doi.org/10.1073/pnas.1917673117, 2020.

Lazar, B. and Stein, M.: Freshwater on the route of hominids out of Africa revealed by U-Th in Red Sea corals, Geology, 39, 1067–1070, https://doi.org/https://doi.org/10.1130/g32257.1, 2011.

Ludwig, P. and Hochman, A.: Last glacial maximum hydro-climate and cyclone characteristics in the Levant: a regional modelling perspective, Environmental Research Letters, 17, 014 053, https://doi.org/https://doi.org/10.1088/1748-9326/ac46ea, 2022.

Ludwig, P., Gómez-Navarro, J. J., Pinto, J. G., Raible, C. C., Wagner, S., and Zorita, E.: Perspectives of regional paleoclimate modeling, Annals of the New York Academy of Sciences, 1436, 54–69, https://doi.org/https://doi.org/10.1111/nyas.13865, 2019.

McGarry, S., Bar-Matthews, M., Matthews, A., Vaks, A., Schilman, B., and Ayalon, A.: Constraints on hydrological and paleotemperature variations in the Eastern Mediterranean region in the last 140 ka given by the δD values of speleothem fluid inclusions, Quaternary Science Reviews, 23, 919–934, https://doi.org/https://doi.org/10.1016/j.quascirev.2003.06.020, 2004.

Neugebauer, I., Brauer, A., Schwab, M. J., Waldmann, N. D., Enzel, Y., Kitagawa, H., Torfstein, A., Frank, U., Dulski, P., Agnon, A., et al.: Lithology of the long sediment record recovered by the ICDP Dead Sea Deep Drilling Project (DSDDP), Quaternary Science Reviews, 102, 149–165, https://doi.org/https://doi.org/10.1016/j.quascirev.2014.08.013, 2014.

Ohgaito, R., Yamamoto, A., Hajima, T., O'ishi, R., Abe, M., Tatebe, H., Abe-Ouchi, A., and Kawamiya, M.: PMIP4 experiments using MIROC-ES2L Earth system model, Geoscientific Model Development Discussions, 2020, 1–29, https://doi.org/https://doi.org/10.5194/gmd-14-1195-2021, 2020.

Orland, I. J., He, F., Bar-Matthews, M., Chen, G., Ayalon, A., and Kutzbach, J. E.: Resolving seasonal rainfall changes in the Middle East during the last interglacial period, Proceedings of the National Academy of Sciences, 116, 24 985–24 990, https://doi.org/https://doi.org/10.1073/pnas.1903139116, 2019.

Otto-Bliesner, B. L., Rosenbloom, N., Stone, E. J., McKay, N. P., Lunt, D. J., Brady, E. C., and Overpeck, J. T.: How warm was the last interglacial? New model–data comparisons, Philosophical Transactions of the Royal Society A: Mathematical, Physical and Engineering Sciences, 371, 20130 097, https://doi.org/https://doi.org/10.1098/rsta.2013.0097, 2013.

Otto-Bliesner, B. L., Brady, E. C., Zhao, A., Brierley, C. M., Axford, Y., Capron, E., Govin, A., Hoffman, J. S., Isaacs, E., Kageyama, M., et al.: Large-scale features of Last Interglacial climate: results from evaluating the lig127k simulations for the Coupled Model Intercomparison Project (CMIP6)–Paleoclimate Modeling Intercomparison Project (PMIP4), Climate of the Past, 17, 63–94, https://doi.org/https://doi.org/10.5194/cp-17-63-2021, 2021.

Palchan, D., Stein, M., Goldstein, S. L., Almogi-Labin, A., Tirosh, O., and Erel, Y.: Synoptic conditions of fine-particle transport to the last interglacial Red Sea-Dead Sea from Nd-Sr compositions of sediment cores, Quaternary Science Reviews, 179, 123–136, https://doi.org/https://doi.org/10.1016/j.quascirev.2017.09.004, 2018.

Petit-Maire, N., Carbonel, P., Reyss, J.-L., Sanlaville, P., Abed, A., Bourrouilh, R., Fontugne, M., and Yasin, S.: A vast Eemian palaeolake in Southern Jordan (29 N), Global and Planetary Change, 72, 368–373, https://doi.org/https://doi.org/10.1016/j.gloplacha.2010.01.012, 2010.

Rohling, E., Cane, T., Cooke, S., Sprovieri, M., Bouloubassi, I., Emeis, K., Schiebel, R., Kroon, D., Jorissen, F., Lorre, A., et al.: African monsoon variability during the previous interglacial maximum, Earth and Planetary Science Letters, 202, 61–75, https://doi.org/https://doi.org/10.1016/s0012-821x(02)00775-6, 2002.

Rosenberg, Thoma, M., Preusser, Fra, n., Risberg, J., Plikk, A., Kadi, K. A., Matter, A., and Fleitmann, D.: Middle and Late Pleistocene humid periods recorded in palaeolake deposits of the Nafud desert, Saudi Arabia, Quaternary Science Reviews, 70, 109–123, https://doi.org/https://doi.org/10.1016/j.quascirev.2013.03.017, 2013.

Rubin, S., Ziv, B., and Paldor, N.: Tropical plumes over eastern North Africa as a source of rain in the Middle East, Monthly Weather Review, 135, 4135–4148, https://doi.org/https://doi.org/10.1175/2007mwr1919.1, 2007.

Saaroni, H., Halfon, N., Ziv, B., Alpert, P., and Kutiel, H.: Links between the rainfall regime in Israel and location and intensity of Cyprus lows, International Journal of Climatology: A Journal of the Royal Meteorological Society, 30, 1014–1025, https://doi.org/https://doi.org/10.1002/joc.1912, 2010.

Schwarcz, H. P., Grün, R., Vandermeersch, B., Bar-Yosef, O., Valladas, H., and Tchernov, E.: ESR dates for the hominid burial site of Qafzeh in Israel, Journal of Human Evolution, 17, 733–737, https://doi.org/https://doi.org/10.1016/0047-2484(88)90063-2, 1988.

Seager, R., Naik, N., and Vecchi, G. A.: Thermodynamic and dynamic mechanisms for large-scale changes in the hydrological cycle in response to global warming, Journal of climate, 23, 4651–4668, https://doi.org/https://doi.org/10.1175/2010jcli3655.1, 2010.

Seager, R., Osborn, T. J., Kushnir, Y., Simpson, I. R., Nakamura, J., and Liu, H.: Climate variability and change of Mediterranean-type climates, Journal of Climate, 32, 2887–2915, https://doi.org/https://doi.org/10.1175/jcli-d-18-0472.1, 2019.

Seland, Ø., Bentsen, M., Graff, L. S., Olivié, D., Toniazzo, T., Gjermundsen, A., Debernard, J. B., Gupta, A. K., He, Y., Kirkevåg, A., et al.: The Norwegian earth system model, noresm2–Evaluation of thecmip6 deck and historical simulations, (No Title), https://doi.org/https://doi.org/10.5194/gmd-2019-378, 2020.

Shi, X., Yang, H., Danek, C., and Lohmann, G.: AWI AWI-ESM1.1LR model output prepared for CMIP6 PMIP, https://doi.org/10.22033/ESGF/CMIP6.9302, 2020.

Sidorenko, D., Goessling, H. F., Koldunov, N., Scholz, P., Danilov, S., Barbi, D., Cabos, W., Gurses, O., Harig, S., Hinrichs, C., et al.: Evaluation of FESOM2. 0 coupled to ECHAM6. 3: preindustrial and HighResMIP simulations, Journal of Advances in Modeling Earth Systems, 11, 3794–3815, https://doi.org/https://doi.org/10.1029/2019ms001696, 2019.

Tibshirani, R. J. and Efron, B.: An introduction to the bootstrap, Monographs on statistics and applied probability, 57, 1–436, https://doi.org/https://doi.org/10.1007/978-1-4842-2382-6_2, 1993.

Tierney, J. E., Torfstein, A., and Bhattacharya, T.: Late Quaternary hydroclimate of the Levant: The leaf wax record from the Dead Sea, Quaternary Science Reviews, 289, 107 613, https://doi.org/https://doi.org/10.1016/j.quascirev.2022.107613, 2022.

Torfstein, A.: Climate cycles in the southern Levant and their global climatic connections, Quaternary Science Reviews, 221, 105 881, https://doi.org/https://doi.org/10.1016/j.quascirev.2019.105881, 2019.

Torfstein, A.: The quaternary climate of Israel, in: Landscapes and landforms of Israel, pp. 49–71, Springer, https://doi.org/10.1007/978-3-031-44764-8_4, 2024.

Torfstein, A., Goldstein, S. L., Kagan, E. J., and Stein, M.: Integrated multi-site U–Th chronology of the last glacial Lake Lisan, Geochimica et Cosmochimica Acta, 104, 210–231, https://doi.org/https://doi.org/10.1016/j.gca.2012.11.003, 2013.

Torfstein, A., Goldstein, S. L., Kushnir, Y., Enzel, Y., Haug, G., and Stein, M.: Dead Sea drawdown and monsoonal impacts in the Levant during the last interglacial, Earth and Planetary Science Letters, 412, 235–244, https://doi.org/https://doi.org/10.1016/j.epsl.2014.12.013, 2015.

Tsvieli, Y. and Zangvil, A.: Synoptic climatological analysis of'wet'and'dry'Red Sea Troughs over Israel, International Journal of Climatology, 25, 1997–2016, https://doi.org/https://doi.org/10.1002/joc.1232, 2005.

Tsvieli, Y. and Zangvil, A.: Synoptic climatological analysis of Red Sea Trough and non-Red Sea Trough rain situations over Israel, Advances in Geosciences, 12, 137–143, https://doi.org/https://doi.org/10.5194/adgeo-12-137-2007, 2007.

Vaks, A., Bar-Matthews, M., Ayalon, A., Schilman, B., Gilmour, M., Hawkesworth, C. J., Frumkin, A., Kaufman, A., and Matthews, A.: Paleoclimate reconstruction based on the timing of speleothem growth and oxygen and carbon isotope composition in a cave located in the rain shadow in Israel, Quaternary Research, 59, 182–193, https://doi.org/https://doi.org/10.1016/s0033-5894(03)00013-9, 2003.

Vaks, A., Bar-Matthews, M., Ayalon, A., Matthews, A., Frumkin, A., Dayan, U., Halicz, L., Almogi-Labin, A., and Schilman, B.: Paleoclimate and location of the border between Mediterranean climate region and the Saharo–Arabian Desert as revealed by speleothems from the northern Negev Desert, Israel, Earth and Planetary Science Letters, 249, 384–399, https://doi.org/https://doi.org/10.1016/j.epsl.2006.07.009, 2006.

Vaks, A., Bar-Matthews, M., Ayalon, A., Matthews, A., Halicz, L., and Frumkin, A.: Desert speleothems reveal climatic window for African exodus of early modern humans, Geology, 35, 831–834, https://doi.org/https://doi.org/10.1130/g23794a.1, 2007.

Vaks, A., Bar-Matthews, M., Matthews, A., Ayalon, A., and Frumkin, A.: Middle-Late Quaternary paleoclimate of northern margins of the Saharan-Arabian Desert: reconstruction from speleothems of Negev Desert, Israel, Quaternary Science Reviews, 29, 2647–2662, https://doi.org/https://doi.org/10.1016/j.quascirev.2010.06.014, 2010.

Waldmann, N., Stein, M., Ariztegui, D., and Starinsky, A.: Stratigraphy, depositional environments and level reconstruction of the last interglacial Lake Samra in the Dead Sea basin, Quaternary Research, 72, 1–15, https://doi.org/doi:10.1016/j.yqres.2009.03.005, 2009.

Waldmann, N., Torfstein, A., and Stein, M.: Northward intrusions of low-and mid-latitude storms across the Saharo-Arabian belt during past interglacials, Geology, 38, 567–570, https://doi.org/https://doi.org/10.1130/G30654.1, 2010.

Yeung, N. K.-H., Menviel, L., Meissner, K. J., Taschetto, A. S., Ziehn, T., and Chamberlain, M.: Land–sea temperature contrasts at the Last Interglacial and their impact on the hydrological cycle, Climate of the Past, 17, 869–885, https://doi.org/https://doi.org/10.5194/cp-17-869-2021, 2021.

Zhang, Q., Li, Q., Zhang, Q., Berntell, E., Axelsson, J., Chen, J., Han, Z., de Nooijer, W., Lu, Z., Wyser, K., et al.: Simulating the mid-Holocene, last interglacial and mid-Pliocene climate with EC-Earth3-LR, Geoscientific Model Development Discussions, 2020, 1–26, https://doi.org/https://doi.org/10.5194/gmd-14-1147-2021, 2020a.

Zhang, Q., Li, Q., Zhang, Q., Berntell, E., Axelsson, J., Chen, J., Han, Z., de Nooijer, W., Lu, Z., Wyser, K., et al.: Simulating the mid-Holocene, last interglacial and mid-Pliocene climate with EC-Earth3-LR, Geoscientific Model Development Discussions, 2020, 1–26, https://doi.org/https://doi.org/10.5194/gmd-14-1147-2021, 2020b.

Zhang, Z., Bentsen, M., Olivié, D. J. L., Seland, Ø., Toniazzo, T., Gjermundsen, A., Graff, L. S., Debernard, J. B., Gupta, A. K., He, Y., et al.: NCC NorESM2-LM model output prepared for CMIP6 PMIP lig127k, 2019.

Zheng, W., Yu, Y., Luan, Y., Zhao, S., He, B., Dong, L., Song, M., Lin, P., and Liu, H.: CAS-FGOALS Datasets for the Two Interglacial Epochs of the Holocene and the Last Interglacial in PMIP4, Advances in Atmospheric Sciences, 37, 1034–1044, https://doi.org/https://doi.org/10.1007/s00376-020-9290-8, 2020.

Ziehn, T., Chamberlain, M. A., Law, R. M., Lenton, A., Bodman, R. W., Dix, M., Stevens, L., Wang, Y.-P., and Srbinovsky, J.: The Australian earth system model: ACCESS-ESM1. 5, Journal of Southern Hemisphere Earth Systems Science, 70, 193–214, https://doi.org/https://doi.org/10.1071/es19035, 2020.

Ziv, B.: A subtropical rainstorm associated with a tropical plume overAfrica and the Middle-East, Theoretical and Applied Climatology, 69, 91–102, https://doi.org/https://doi.org/10.1007/s007040170037, 2001.

Ziv, B., Shimer, R., Harpaz, T., Drori, R., Alpert, P., Raveh-Rubin, S., and Saaroni, H.: Identification and classification of the wet Red Sea Trough over Israel, International Journal of Climatology, 42, 10 062–10 082, https://doi.org/https://doi.org/10.1002/joc.7884, 2022.

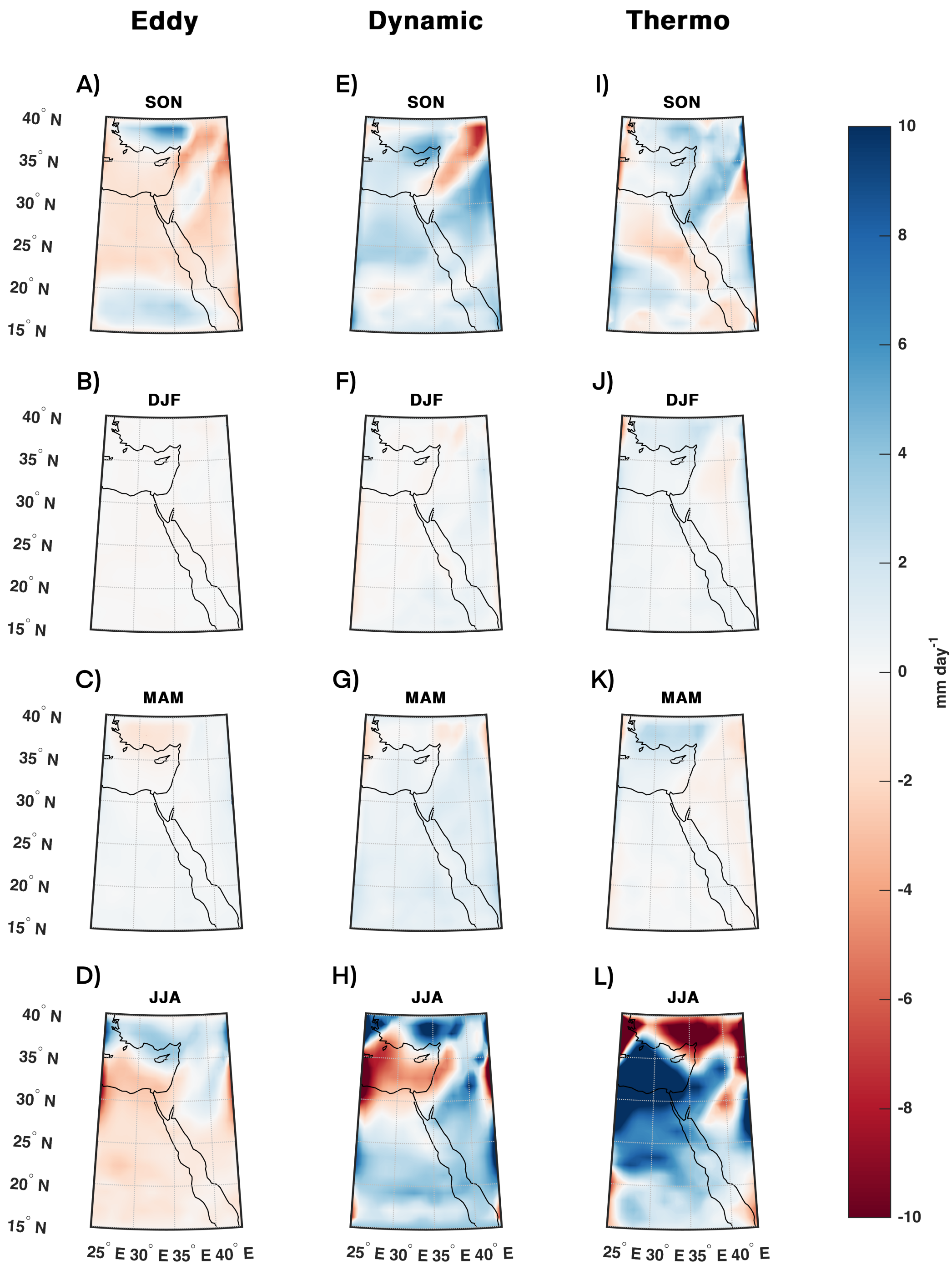

Figure 6. Eddy, Dynamic and Thermodynamic (Thermo) decomposition of the difference between Precipitation - Evaporation $\Delta P - E$ [mm/d] in the LIG peak compared to the PI period. For every season: Autumn [SON, A - C], Winter [DJF, D - F], Spring [MAM, G - I], and Summer [JJA, J - L]. Multi-model ensemble mean of the nine PMIP4 models. Colored regions denote statistically significant changes at the 95% level as determined by a bootstrap test.